

*Citation for published version:*

Swart, B, Zhao, Y, Khaku, M, Che, E, Maltby, R, Chew, YMJ & Wenk, J 2020, 'In situ characterisation of size distribution and rise velocity of microbubbles by high-speed photography', *Chemical Engineering Science*, vol. 225, 115836. <https://doi.org/10.1016/j.ces.2020.115836>

*DOI:*

[10.1016/j.ces.2020.115836](https://doi.org/10.1016/j.ces.2020.115836)

*Publication date:*

2020

*Document Version*

Peer reviewed version

[Link to publication](#)

*Publisher Rights*

CC BY-NC-ND

**University of Bath**

## **Alternative formats**

If you require this document in an alternative format, please contact:  
[openaccess@bath.ac.uk](mailto:openaccess@bath.ac.uk)

**General rights**

Copyright and moral rights for the publications made accessible in the public portal are retained by the authors and/or other copyright owners and it is a condition of accessing publications that users recognise and abide by the legal requirements associated with these rights.

**Take down policy**

If you believe that this document breaches copyright please contact us providing details, and we will remove access to the work immediately and investigate your claim.

# *In situ* characterisation of size distribution and rise velocity of microbubbles by high-speed photography

Bert Swart<sup>a,b</sup>, Yubin Zhao<sup>a</sup>, Mohammed Khaku<sup>a</sup>, Eric Che<sup>a</sup>, Richard Maltby<sup>a,c</sup>, Y.M. John

Chew<sup>a,d\*</sup>, Jannis Wenk<sup>a,b\*</sup>

Keywords: Bubble size distribution, Image processing, Microbubbles, Rise velocity, Surfactants

<sup>a</sup> Department of Chemical Engineering, University of Bath, Bath, BA2 7AY, United Kingdom.

<sup>b</sup> Water Innovation and Research Centre, University of Bath, BA27AY, UK

<sup>c</sup> Centre for Sustainable Chemical Technologies, University of Bath, Bath BA2 7AY, UK

<sup>d</sup> Centre for Advanced Separations Engineering, University of Bath, Bath BA2 7AY, UK

\* Corresponding authors:

John Chew, Centre for Advanced Separations Engineering,  
Department of Chemical Engineering, University of Bath, Bath BA2 7AY, UK.  
email: y.m.chew@bath.ac.uk  
phone: +44 (0) 1225 38613

Jannis Wenk, Water Innovation and Research Centre,  
Department of Chemical Engineering, University of Bath, Bath BA2 7AY, UK.  
email: j.h.wenk@bath.ac.uk  
phone: +44 (0) 1225 384469

Number of pages 34.

Number of figures 12.

Number of tables: 2.

Number of words (excluding title page, captions and references): 5840.

## Abstract

Using microbubbles has gained significant interest in many domestic and industrial applications due to bubble stability in solution and increased mass transfer area. The characterisation of microbubble populations is therefore important and aids in the understanding of their behaviour. Microbubble characterisation remains challenging, particularly at high bubble densities. We have developed an in situ and automated method, based on image analysis, to determine bubble size distributions and bubble rise velocity at bubble densities of up to approximately 7 bubbles mm<sup>-2</sup>. The method uses image analysis of a side-stream viewing slit and was tested using air bubbles in water at diameters between 20 and 150 µm under a range of different conditions. The developed system enables fast, simple and accurate size determination for microbubbles, including continuous sampling and observation.

## 1. Introduction

Bubbles are essential in two-phase (gas-liquid) and three phase (gas-liquid-solid) contacting in processing industries for example in aeration, flotation, absorption, fluidisation and distillation [1]–[6]. Bubble size and precise control of its distribution are central information in characterising processes, but is challenging given the complex relationship between bubble shape, size, movement and surrounding forces. Bubbles fall into different size categories. Macrobubbles, also referred to as millibubbles, are typically between 2-5 mm in diameter [2]. ISO/TC 281 defines a bubble as ‘*gas in a medium enclosed by an interface*’ and specifies bubbles of a volume equivalent diameter less than 100 µm as fine bubbles, while distinguishing between microbubbles (MBs, 1-100 µm) and ultrafine bubbles (< 1 µm). The term ‘ultrafine bubble’ is favoured over the frequently used term ‘nanobubble’ due to the unclear definition of the latter term [7]. Given the various size range definitions for bubbles in the literature [3], [8], [9], the present study uses ISO terms and definitions.

Due to their hydrodynamic properties MBs are used extensively in water clarification and solids removal processes, such as dissolved air flotation (DAF) [10]–[13]. Other applications include ozonation, removal of pesticides, disinfection, removal of oil, airlift bioreactors, aeration in aerobic activated sludge treatment, sludge solubilisation in biological water treatment and degreasing of solid surfaces [2], [14]–[19]. MBs have very large surface to volume ratios in the order of 10<sup>5</sup> m<sup>2</sup>

<sup>1</sup> resulting in surface forces such as surface tension and skin drag dominating over inertial forces. MBs also do not coalesce and break up in the same way as larger bubbles, which is thought to be due to repulsive forces caused by negative surface charge. High bubble density, large surface area and long residence time provide effective contacting between bubbles and particles in the surrounding liquid and decreased propensity of detachment from particles due to lower inertia [10], [20]–[28]. The highly stable nature of MBs in solution also make them particularly suited to aeration [29]–[31]. The stability and low rise velocities of MBs result in high residence times, allowing MBs to shrink and dissolve in unsaturated water prior to reaching the liquid surface.

Reviews on bubble formation and bubble hydrodynamics cover rise velocity, coalescence, breakup and the various bubble interactions [6], [32]. Literature on MBs in particular, is related to its use for aeration processes and DAF. DAF MB research covers bubble-bubble/bubble-particle interactions, the effect of bubble characteristics such as size, hydrophobicity, zeta potential and the internal and external hydrodynamic behaviour of microbubbles which are determined by the fluid properties and bubble morphology [33]–[40]. Other research has focused on the effect of surfactants on the behaviour of MBs [41]–[45]. Computational fluid dynamics (CFD) modelling has been utilised to understand the flow around MBs and specifically the effect of MB size and density on flows within DAF tanks [46]–[51].

There are various bulk generation methods for MBs which fall into two categories, (1) gas-water circulation/shear force and (2) pressurisation/depressurisation [2]. In gas-water circulation, MBs are generated via breakup by flow turbulence and vortices. In pressurisation/depressurisation, MBs are produced by first supersaturating liquid with gas at high pressure, and subsequently reducing the pressure. Another method, which utilizes pressure drop, is hydrodynamic cavitation, in which a localised area of decreased pressure causes the nucleation of gas bubbles. Usually, for DAF pressurisation/depressurisation is applied. Water is saturated with air at 0.4-0.6 MPa and then passed through injection nozzles over which a pressure drop occurs resulting in the formation of MBs in the 40-150  $\mu\text{m}$  range [10], [13], [52], [53]. The major drawback with the pressurisation/depressurisation method of MB generation is the need for large pressurisation tanks and the high operating costs involved in pressurising the recycle stream. Different MB generators include spiral liquid, Venturi and ejector type generators [18]. Venturi and ejector type generators utilise hydrodynamic cavitation via pressure changes in flow channels, with the Venturi type

generating bubbles of 1-60  $\mu\text{m}$  [18], [54]. Spiral liquid type generators generate bubbles of 10-50  $\mu\text{m}$  via shear forces generated by centrifugation [55]. A fluidic oscillator type MB generator to produced bubbles of 40-250  $\mu\text{m}$  [56].

Table 1 shows the various methods employed to characterise MB size distributions and rise velocities. The critical steps in bubble characterisation experiments are (1) the acquisition of bubbly liquid samples, (2) the measurement of bubble size and rise velocity and (3) data analysis. While imaging methods have been most widely used, other techniques include light diffraction, drift flux analyses, porous plate, electro resistivity and optical detectors. Data analysis ranges from measuring the size of individual bubbles manually to sophisticated automated methods, which for example can determine bubble sizes within clusters. Most rise velocity measurements employed high-speed photography followed by image analysis. For example, some studies observed isolated individual bubbles using image sequences [42], [57], [58]. Other studies looked at the rise-velocity of bubble-floc agglomerates using commercial imaging software [59] or conducted measurements of individual bubbles using laser velocimetry [60].

Here we describe a new MB analytical setup that can measure microbubble sizes and size distributions, including single bubble and population size rise velocities at relatively high bubble densities of approximately 7 bubbles per  $\text{mm}^2$ , with images of up to 100 bubbles per frame analysed. Bubbles were produced in pure water using a NIKUNI KTM20 regenerative turbine pump at different temperatures and with/without the presence of surfactants. Bubble solution was directed from the MB generator into a viewing slit where images were captured, followed by digitalised image analysis. This setup is relatively low cost and enables *in situ* (via a side stream), direct and continuous sampling of bubbles without altering the operation of the MB generator. Automated imaging analysis was developed in MATLAB to enable fast and detailed characterisation of dense populations of bubble diameters and rise velocity in pure water and water charged with surfactants.

111 **Table 1:** Summary of bubble size and rise velocity characterisation methods.

Bubble Size				
Experimental Setup	Measurement	Analysis	Size Range	Reference
Samples drawn into laser online particle counter	Light diffraction (Chemtrac PC2400 D, USA)	Conversion of diffraction to bubble size	15-85 $\mu\text{m}$	[61]
Samples drawn into batch type particle counter	Electrical resistivity (Multisizer II, Coulter)	Conversion of resistivity to bubble size	13-96 $\mu\text{m}$	[61]
Samples tapped into Perspex viewing cell (0.08 m, 0.08m and 0.015 m)	Photography	Image analysis software <i>Image-Pro plus</i>	10-150 $\mu\text{m}$	[30]
Lab scale DAF unit with samples drawn into viewing chamber.	Digital camera & backlighting	Bubble size analyser software <i>LabVIEW</i> (BASF)	60-131 $\mu\text{m}$	[62]
Samples from DAF unit tapped off into cuvette	Photography	Automatic image analysis <i>Magiscan</i> (Joyce Loebel)	10-300 $\mu\text{m}$	[63]
Bubbles generated by diffusers in tank	Acoustic spectrometry	Analysis of signals obtained by acoustic bubble spectrometer system using software	80-500 $\mu\text{m}$	[56]
Pilot flotation column	Gas velocity and gas holdup	Drift flux analysis	350-1100 $\mu\text{m}$	[64]
Lab scale flotation unit	Digital camera	Stochastic image analysis incorporating bubble clusters	200-2000 $\mu\text{m}$	[65]
Flotation cell	Digital camera	Image analysis software <i>Matrox Inspector</i>	500-3000 $\mu\text{m}$	[66]
McGill bubble size analyser (sampling tube & tilted viewing chamber)	Digital camera	One dimensional discrete Fourier analysis	500-5000 $\mu\text{m}$	[67]
Bubble Rise Velocity				
Experimental Setup	Measurement	Analysis	Size Range/Rise Velocity Range	Reference
Single bubbles transferred into a cuvette	High speed camera	Manual image analysis	10-120 $\mu\text{m}$ 1-12 $\text{mm s}^{-1}$	[57]
Single bubbles generated in electrophoresis cell	Photodetector	Laser Doppler velocimetry	$\approx 80 \mu\text{m}$ 4-5 $\text{mm s}^{-1}$	[60]
Carried out batch flotation of bubble-particle flocs in jar tester	High speed camera	Particle image analyser software	200-700 $\mu\text{m}$ (Floc) 9-15 $\text{mm s}^{-1}$	[59]
Single bubbles transferred into a viewing chamber	High speed camera	MATLAB image analysis	1300-2000 $\mu\text{m}$ 200-500 $\text{mm s}^{-1}$	[58]
Downward flow chamber used to isolate a bubble and keep stationary relative to camera with flow stopped periodically for velocity determination	High speed camera	Manual analysis using known distance travelled	1000-5000 $\mu\text{m}$ 100-350 $\text{mm s}^{-1}$	[42]

## 2. Theory

Precise control and knowledge of bubble size is critical in determining gas-liquid flow regimes. A series of dimensionless numbers are commonly used to characterise bubbles in terms of shape and flow regime. The Reynolds number ( $Re_b$ , equation (1)) describes the ratio of inertial to viscous force, the Eötvös number ( $Eo$ , equation (2)) is the ratio of gravitational force to surface tension, and the Morton number ( $Mo$ , equation (3)) is a constant for a given liquid and gas mixture at constant temperature and is used in conjunction with  $Eo$  to determine the shape of the bubble. The shape of bubbles moving in a fluid can be predicted by utilising a plot, called the Grace diagram, incorporating all three dimensionless numbers [68].

$$Re_b = \frac{\rho_l u_b D_b}{\mu_l} \quad (1)$$

$$Eo = \frac{\Delta \rho g D_b^2}{\gamma} \quad (2)$$

$$Mo = \frac{g \mu_l^4 \Delta \rho}{\rho_l^2 \gamma^3} \quad (3)$$

Larger macrobubbles rise faster due to a lower surface to volume ratio and reduced drag, and therefore result in higher  $Re_b$ . Regardless of the  $Mo$  number, bubbles are spherical under gravitational motion through a fluid when  $Re_b < 1$ , and/or when  $Eo < 0.2$  (air bubble in water with  $D_b < 1.2$  mm). When surface tension is large enough, bubbles remain spherical up to  $Re_b < 600$ . When bubbles exhibit little internal circulation, then flow around a bubble can be described in the same way as for solid spherical particles. There are several correlations for the drag coefficient of spheres, which approximate the drag coefficients given by the standard drag curve [69]. When internal circulation is present the dynamics of rising bubble through liquid becomes more complex and relies mostly on numerical methods [70].

For bubbles with  $Re_b < 1$ , the flow around the bubble is classified as creeping flow, therefore Stokes' law (Eq. 4) can describe the rise velocity of an isolated bubble. The Hadamard-Rybczynski (H-R) equation (Eq. 5) applies for a bubble with a mobile surface and internal circulation [71].

$$u_{t(ST)} = \frac{D_b^2 \Delta \rho g}{18 \mu_l} \quad (4)$$

$$(5)$$

$$u_{t(H-R)} = \frac{D_b^2 \Delta \rho g}{6\mu} \frac{\mu_l + \mu_g}{2\mu_l + 3\mu_g}$$

One criteria used to predict the behaviour of MBs is the Bond criterion [72], which states that for  $Eo < 4$  there is no internal circulation within rising bubbles [73].

$$Eo = \frac{D_b^2 \Delta \rho g}{\gamma} \begin{array}{l} > 4 \text{ Fluid Behaviour} \\ < 4 \text{ Solid Behaviour} \end{array} \quad (6)$$

However it is well known from experimental observation that bubbles deviate from the Bond criterion due to the presence of surface active substances which immobilise the bubble surface [41]. This immobilisation occurs due to an accumulation of surface contaminants at the rear of a moving bubble; creating a surface tension gradient that opposes viscous stress at the surface. This phenomenon is known to occur more easily with microbubbles even with trace quantities of contaminants and can only be avoided by using ultra-pure water [42], [57]. Further correlations have been developed to predict the rise velocity in different scenarios for example for bubble-particles flocs present at low and high  $Re_b$  numbers [10], [73]–[75]. For spherical particles at  $Re_b > 1$  Clift *et al.* [70] present a summary of recommended drag coefficients (Table 2). At  $Re_b < 10$ , however, the deviation of the drag coefficient  $C_d$  from Stokes' law is no more than twice the Stokes' drag, which corresponds to a maximum reduction in rise velocity of 30% from that predicted by Stokes' law. Clift *et al.* [71] also present drag coefficients for slow viscous flow past spheres using extensions of the creeping flow solution such as Oseen's approximations. These extensions were developed because the creeping flow solutions are only valid for distances less than  $D_b/2Re_b$  from the sphere. In addition to the rise velocity for an individual bubble, the effect of multiple bubbles in a bubble population on rise velocity has also been considered [76]. Simulations have shown that at low volume fractions, cooperative wake interactions lead to an increase in rise velocity. However, at higher volume fractions hindering viscous forces begin to dominate and reduce the rise velocity. Based on the Eotvos/Bond numbers used for spherical bubbles, these simulations were based on bubbles with diameters between 1.5 and 2 mm for air/water bubbles.



**Table 2:** Correlations for the drag coefficient of a sphere moving slowly through a viscous fluid according to Stokes' law, the Oseen extension and a modified Oseen extension as well as correlations for drag at Reynolds numbers above 1. [70], [71].

Correlation		Range
$C_{DST} = \frac{24}{Re_b}$	(7)	$Re_b < 1$ , Stokes' Law
$C_D = \frac{24}{Re_b} \left[ 1 + \frac{3}{16} Re_b \right]$	(8)	$Re_b < 0.1$ , Oseen's approximation
$\frac{C_D}{C_{DST}} - 1 = \frac{3c}{16} Re_b, \quad c = 0.43$	(9)	$Re_b < 1$ , Modified Oseen's approximation
$\log_{10} \left[ \frac{C_D Re_b}{24} - 1 \right] = -0.881 + 0.82w - 0.05w^2$	(10)	$0.01 < Re_b \leq 20$
$\log_{10} \left[ \frac{C_D Re_b}{24} - 1 \right] = -0.7133 + 0.6305w$	(11)	$20 \leq Re_b \leq 260$
$\log_{10} C_D = 1.6435 - 1.1242w + 0.1558w^2$	(12)	$260 \leq Re_b \leq 1500$

### 3. Materials and methods

#### Method of MB generation

A NIKUNI KTM 20N (Nikuni Co., Kawasaki City, Kanagawa, Japan; Aeration & Mixing LTD, Sheffield, UK) regenerative turbine pump was used in all experiments to produce MBs. The pump has a liquid and gas inlet with control of both streams, allowing variation of gas liquid ratio in the pump. The Nikuni KTM design harnesses three forces in a single stage pump. A frictional force directing flow in the direction of impeller rotation, an axial force pushes fluid present in the pump either side of the centre of the impeller into the chambers and centrifugal force encourages fluid to swing outwards away from the centre of the impeller towards the side of the pump casting. These forces in combination with the action of the impeller result in a series of vortexes to form, creating areas of low pressure in which air is sheared and becomes entrained forming MBs [77]. Unless otherwise stated, the pump was operated at manufacturer recommended parameters of 0.3 MPa Outlet pressure, -0.03 MPa Inlet pressure, liquid flow rate of 16.5 L min<sup>-1</sup> and an ambient air intake of 1.5 L min<sup>-1</sup> (Figure 1)

#### Temperature controlled flow loop and MB imaging

The following methodology lays out the experimental setup and procedure developed in the investigation of the size distribution and rise velocity of MBs produced under varying operating conditions. Unbuffered deionized (DI) water from an in-house reverse osmosis system was used for all experiments and preparation of stock solutions. Two ionic surfactants; cetyl trimethyl ammonium bromide (CTAB) (CAS-57-09-0), glycolic acid ethoxylate lauryl ether (GAELE) (CAS- 220622-96-8) and two non-ionic surfactants; polyethylene glycol sorbitan monolaurate (Tween-20) (CAS-9005-64-5) and Triton-X-100 (CAS- 9002-93-1) were sourced from *Sigma Aldrich*. All surfactant dosages were calculated based on the critical micelle concentration (CMC) for CTAB, GAELE, Tween 20 and Triton X-100 of 0.92, 0.22, 0.06 and 0.10 mM, respectively (*manufacturer information*). Air microbubbles were generated in a temperature-controlled loop system with a liquid reservoir volume of 30 L. The system was equilibrated at stable desired temperature (10 - 60 °C) for 2 min before measurements were started. Temperature control was carried out using a 6 mm diameter cooling/heating coil with an approximate length of 4 metres. Recycling of liquid resulted in high bubble densities in the closed loop and enabled stream split at the pump outlet, including control of bubble density in the observation unit by adjustment of a needle valve. Solution flowed from the needle valve to the viewing slit along plastic tubing ( $\approx$  30 cm). Solution entry through a perforated bottom (1 mm holes) ensured homogenous bubble distribution in the viewing slit ( $<$  3 mm thick Perspex, 530 mm height  $\times$  110 mm width  $\times$  8 mm depth). Both reservoir loop and viewing slit were cleaned daily and rinsed with DI water followed by the desired surfactant solution for surfactant series experiments.

For each experiment, 200 images were captured with a Thorlabs DCU224C camera (*Thorlabs*, United States) with Navitar 12 $\times$  zoom lens (*Navitar*, United States) at 10 frames per second. The camera was mounted on an adjustable support system to ensure that position and distance from the viewing slit (5-10 cm) could be accurately controlled. A backlight system (*Nightsearcher Galaxy Pro* at 15 cm distance) ensured sufficient contrast. A scale image was taken before each experiment to be used when converting bubble diameters from pixel width to  $\mu$ m. For accurate bubble rise velocity measurements, the needle valve was only opened briefly to allow bubbles into the viewing slit and then shut, with imaging conducted after the dissipation of eddies and flow stratification in viewing slit and free bubble motion was present. The delay required varied on a case by case basis, especially with temperature variation as more turbulence was present at higher temperatures,

although generally it would take no more than 1 minute for the bubble motion to stabilise. Images were captured 30 cm above the slit entrance to minimise entrance effects.

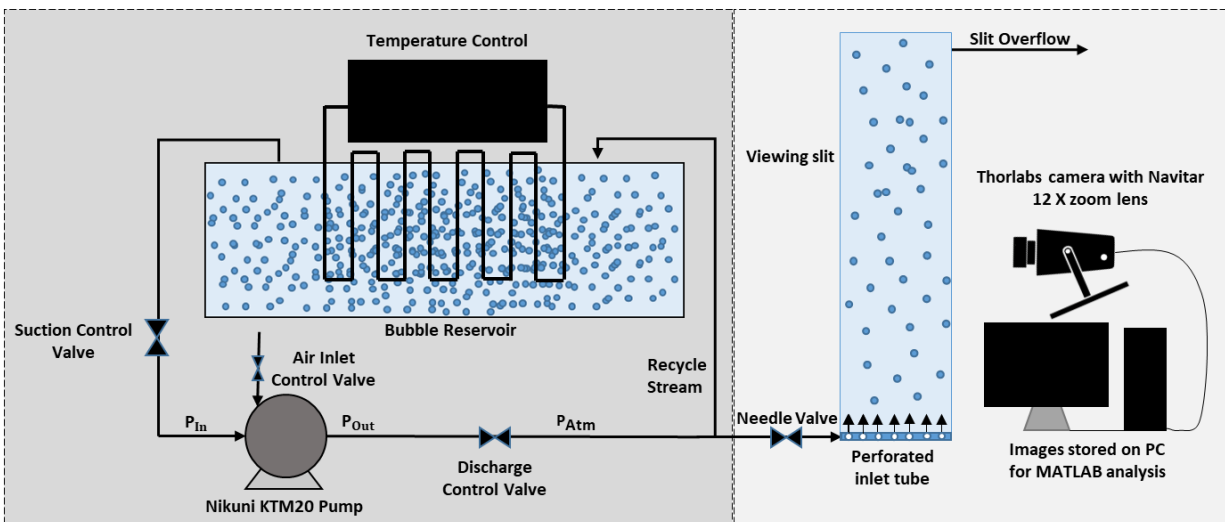


**Figure 1:** Setup of temperature-controlled flow loop and microbubble observation.

## 212 Image Processing

213 A MATLAB (R2018b) (Supporting Information) code for image analysis was developed to  
214 identify the position and diameter of bubbles that are in focus. The identification was based on the  
215 exclusion of image objects based on three factors; threshold binarising via Otsu's method [78],  
216 eccentricity and minimum intensity of object. Binarising the image is used as a means of singling  
217 out bubbles by eliminating background image. This is done by simple exclusion/inclusion decision  
218 based on the darkness of each pixel. Eccentricity is used as a means of excluding/including bubbles  
219 based on the roundness of objects within the image. Minimum intensity is used as a means of  
220 including/excluding objects based on the darkness of each object. For example, out of focus and  
221 smaller bubbles would appear lighter than in focus bubbles. All three parameter thresholds could  
222 be set manually and tested in order to optimise bubble identification. Figures 2(a) and (b) illustrate  
223 how image analysis was used to record bubble size distribution and rise velocity. First, the image  
224 was loaded and converted to a grayscale intensity image and transformed to its complement. The  
225 image was then binarised according to a user-defined threshold based on image contrast and  
226 background brightness (A). The objects in the image were filtered based on eccentricity in order  
227 to eliminate any overlapping bubbles and minimum intensity to eliminate bubbles that were out of  
228 focus (B & C). The minimum intensity filtering step C, is applied by considering the grayscale of  
229 the original image which is actually a negative of the original image. In the MATLAB code the  
230 MinIntensity values were set as 100 minus the MinIntensity. For ease of understanding, the plots  
231 are made using labels of 100-MinIntensity to highlight this flipping of the thresholding logic. For  
232 rise velocity analysis, the code was extended to record the bubble x-coordinate, y-coordinate, mean  
233 intensity and diameter. These four parameters were then used to identify the same bubble in  
234 consecutive images by creating an image link and track bubbles in order to determine rise velocity.  
235 Bubbles would be identified as the same bubble between two consecutive linked images if the  
236 difference of the values of the four parameters fell within specified criteria, a maximum x-  
237 coordinate difference ( $\approx 200 \mu\text{m}$ ), maximum mean intensity difference ( $\approx 2$ ), maximum diameter  
238 difference ( $\approx 2 \mu\text{m}$ ) and maximum y-coordinate difference ( $\approx 1000 \mu\text{m}$ ). Once optimised these  
239 four criteria can remain unchanged. However, the maximum y-coordinate difference may be  
240 changed on a case-by-case basis. For example, when analysing smaller bubbles a lower maximum  
241 y-coordinate setting can account for slower rise velocities and thereby improve accuracy of results.

To avoid false linkage of bubbles between two images, bubbles were eliminated from the analysis if more than one bubble in the second image fell within the specified criteria.

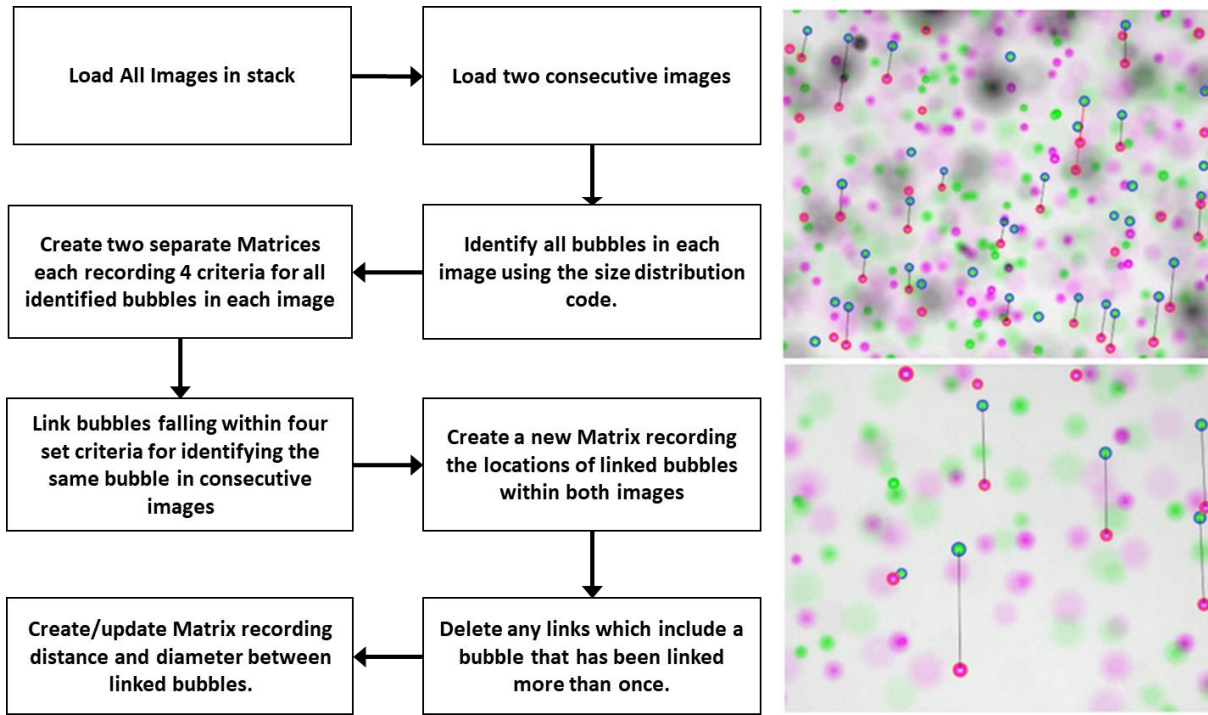
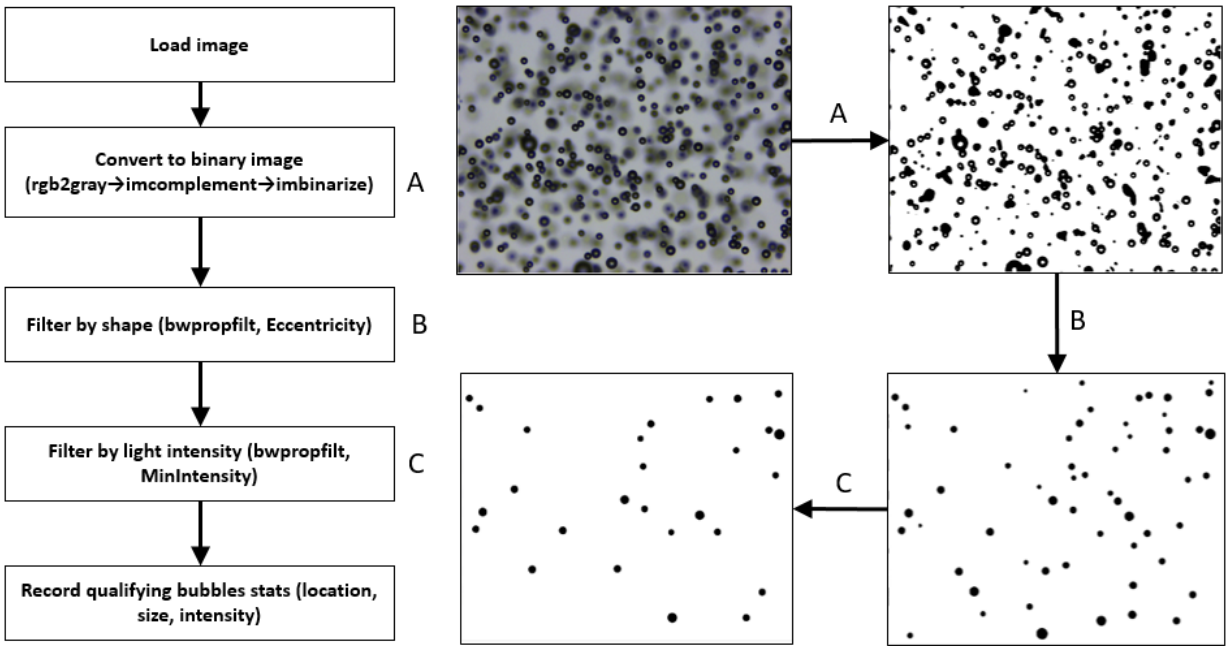


**Figure 2:** (a) Flowchart of the size distribution code procedure along with step images, and (b) flowchart of the rise velocity code procedure along with two examples showing the tracking of bubbles in consecutive images demonstrating the ability to analyse two images with different sized bubbles and bubble density.

To avoid skewing of results by any excessively large and small bubbles within a sample, including false identifications due to image processing error, the 1<sup>st</sup> and 4<sup>th</sup> quartile of the size distribution was not taken into account when calculating mean bubble diameter, shown in Figure 3. Figure 3a shows a cumulative frequency plot of the bubble size distribution and figure 3b shows a normalised plot of the size distribution. Lines are added in both plots to highlight the interquartile range (IQR) and the mean diameter which is calculated using the data within the IQR. The effect of using only the IQR on the obtained mean diameters was investigated and showed differences no bigger than 2.3% compared to analysis using all the data. The results of this analysis can be seen in the supporting information (Figure S2).

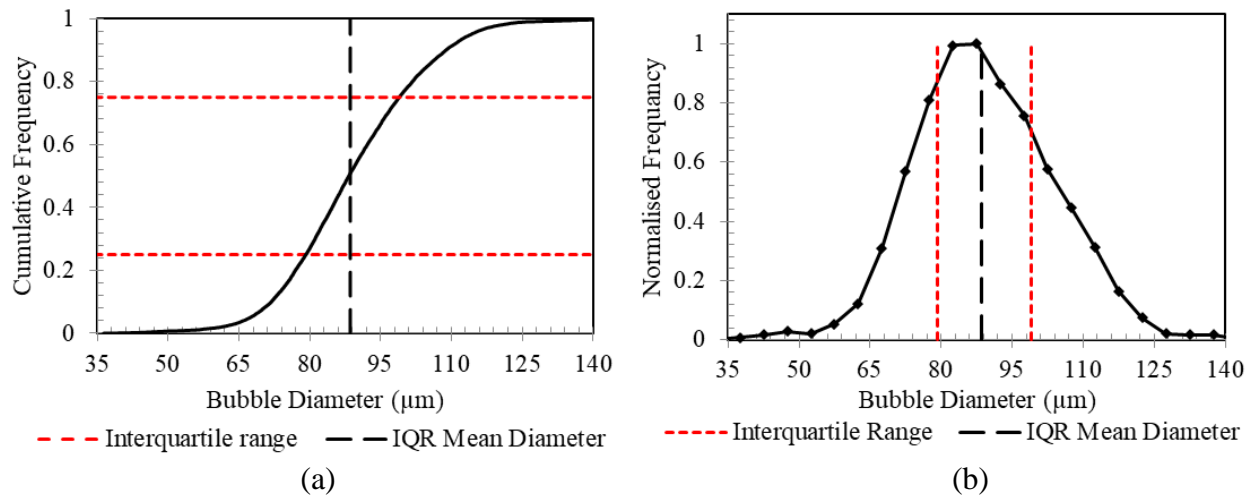


**Figure 3:** Typical size distribution produced by the image analysis showing the interquartile range (IQR) and the IQR mean diameter.

#### 4. Results and discussion

##### Sensitivity analysis and validation of image processing

Obtaining a true measure of accuracy for the described method is difficult as there is no accurate methodology to compare with. In order to maximise accuracy, the effect of sampling on the bubble

size must be minimised. In our case this was done by keeping connecting tubing from pump outlet and viewing slit to a minimum length and diverting at low flow rates so as to minimise turbulent effects which could lead to bubble coalescence or breakup. The second factor which determines accuracy is the image analysis itself. In our case the source of error in identifying and determining MB size lies in the setting of the values for the imbinarise, eccentricity and minimum intensity factors. The parameters initially need to be set by the user within ranges of 0-1 for Imbinarise and Eccentricity and 0-100 for MinIntensity. Figure 4 illustrates the effect of changing the factors for a given image beyond the thresholds at which incorrect bubble inclusion and exclusion could occur. At low Imbinarise threshold i.e. 0.65, dark areas between bubbles and out of focus bubbles would be incorrectly included. At high Imbinarise threshold i.e. 0.85, areas of in focus bubbles would be excluded. At low eccentricity thresholds i.e. 0.2, bubbles were incorrectly excluded and at high thresholds i.e. 0.9, overlapping bubbles were incorrectly included. At high MinIntensity thresholds i.e. 85, smaller bubbles would be disproportionately excluded and at lower thresholds i.e. 60, out of focus bubbles would be incorrectly included and appear smaller than in reality. It was found that outside set ranges for Imbinarise (0.7 - 0.8), Eccentricity (0.3 - 0.8) and 100- MinIntensity( 15- 40), bubbles were either incorrectly excluded, included or incorrectly represented (Figure 4). These ranges are therefore the feasible range for factor settings. Note, factor ranges were determined for specified experimental conditions with clear water and air bubble mixtures. Under different experimental conditions, for example under different lighting conditions, these factors would need to be re-evaluated to optimise bubble identification. Key parameters affected are the Imbinarise and MinIntensity factors, as both build on intensity and brightness of object pixels. For example, Imbinarise values need to be set as low as 0.5 to fully capture bubbles in solution under brighter lighting conditions with backlighting moved closer to the viewing slit. Regardless of the camera used by converting images to grayscale and known scale the code will function properly.

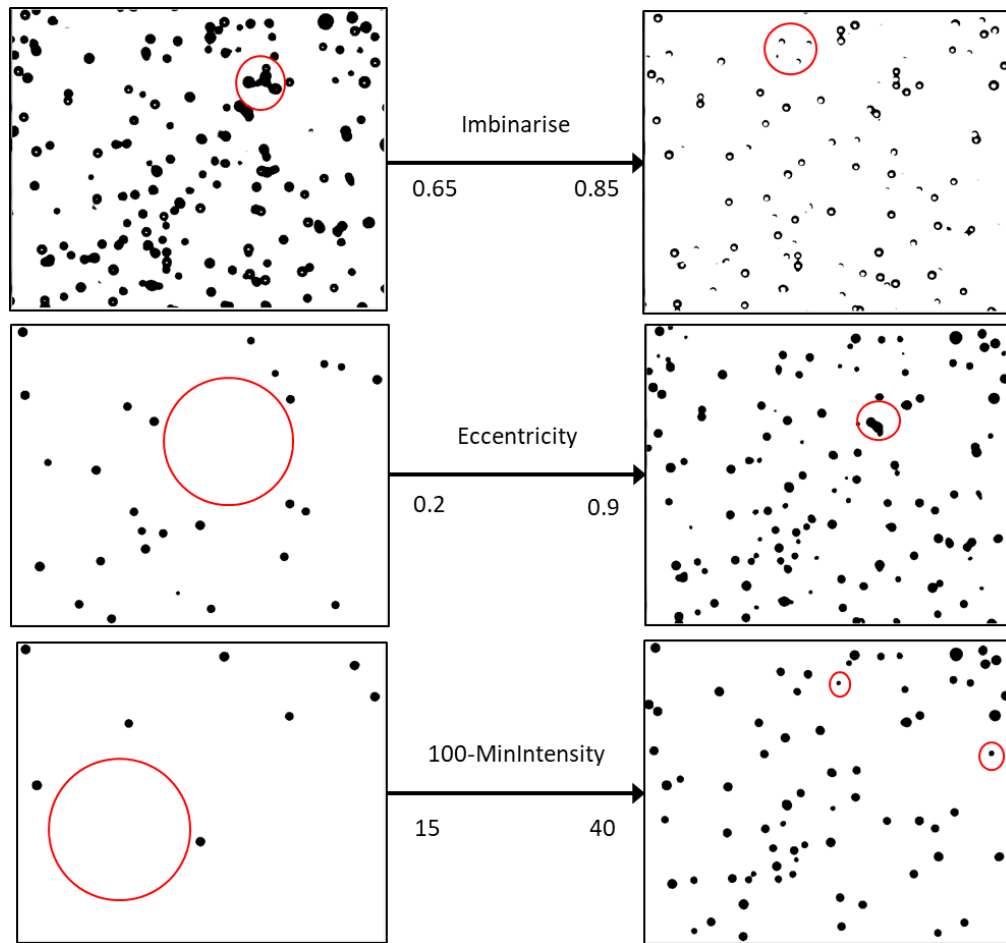


**Figure 4:** Images (3.4 mm × 4.3 mm) showing the effect of varying the factors in the Matlab analysis with baseline settings of Imbinarise = 0.75, Eccentricity = 0.5 and 100-MinIntensity = 25. Red circles highlight incorrect bubble inclusion or exclusion.

A sensitivity analysis was carried out to determine the effect of altering the parameters within the feasible ranges on a single set of 200 images to quantify potential error introduced in the image processing. First, a baseline of parameter values (Imbinarise = 0.75, Eccentricity = 0.5, 100-MinIntensity = 25) was established by utilising visual observation, comparing the original image to the processed image and determining the optimum parameter values. Each parameter was then altered whilst keeping the others constant, recording mean diameter and total number of bubbles identified. Figure 5 shows the results of the sensitivity analysis. Varying the minimum intensity and binarising factor had a larger effect on the perceived mean bubble size than the eccentricity factor, with a total range of only 4  $\mu\text{m}$  when altering the eccentricity factor compared to a range of more than 8  $\mu\text{m}$  when altering minimum intensity and binarising factor.



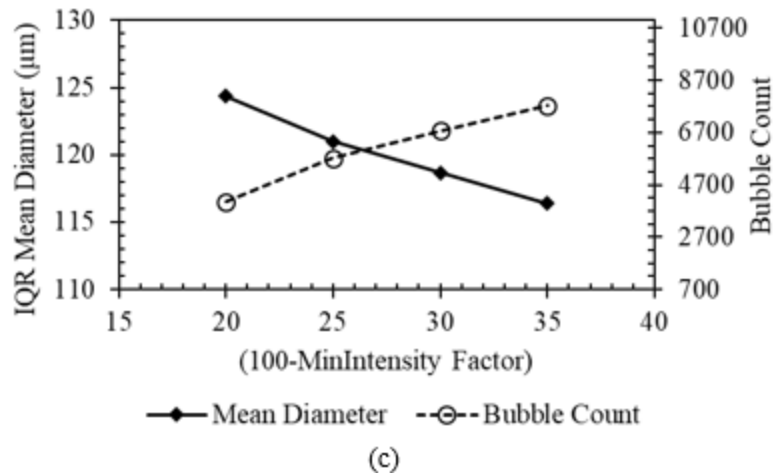
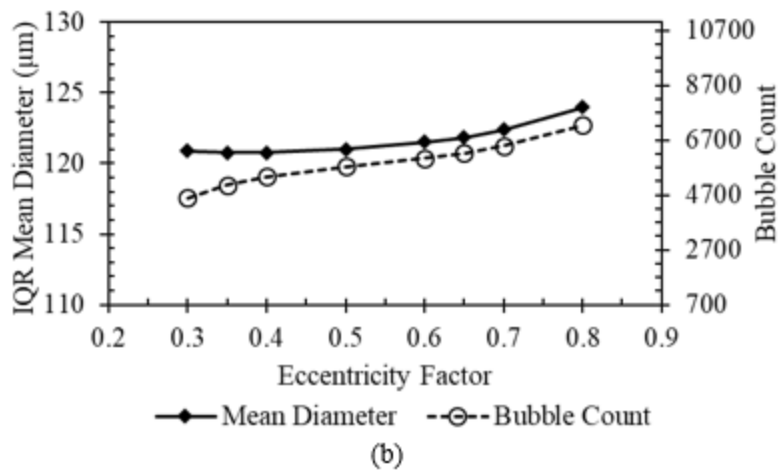
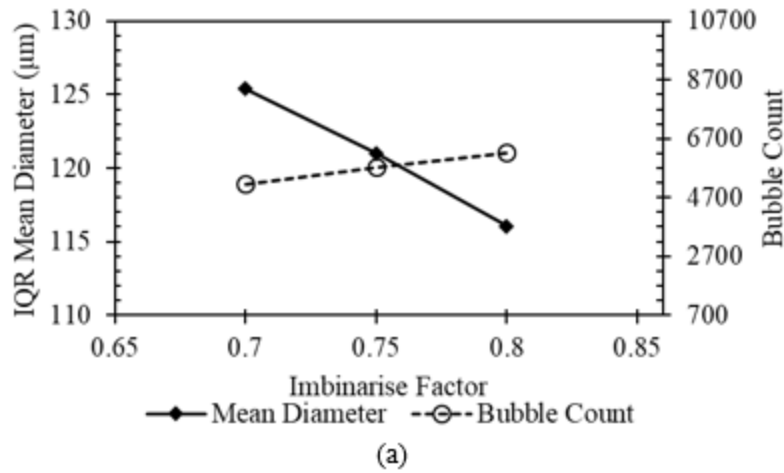


**Figure 5:** Sensitivity analysis on the effects of image processing factors on determined mean bubble size and tracked bubble count. (IQR = interquartile range).

In order to quantify the maximum potential error in mean diameter identification a sensitivity analysis was carried out by testing all possible combinations of the parameters at the extremes

within the feasible range. Full results of this sensitivity can be found in the Supporting Information. The total range in mean diameter obtained from this sensitivity analysis was  $20.7 \mu\text{m}$ , which equates to an error of  $\pm 9.7\%$  from the mean diameter obtained at the set baseline parameter values (Imbinarise = 0.75, Eccentricity = 0.5, 100-MinIntensity = 25). The maximum error in obtaining mean diameter is expected to be less than 10%. However, there is an inherent error introduced due to overlapping bubbles being ignored by the analysis. For bubbles in the millimetre range this can lead to an underestimation of larger bubbles of 7.9% - 11.6% and 2% - 7% after stochastic correction, respectively [65]. For MBs it is unlikely that such underestimation is significant due to their more uniform distribution. In order to validate the image processing technique more than 500 bubbles within a set of seventeen images, from two different experimental runs, were manually sized utilising the Imdistline function on MATLAB. The manual analysis allowed measurement of visible bubbles that would be excluded by the automated method due to overlapping. Due to the rather small number of bubbles analysed, the shape of the size distribution plots in Figure 6(a) are not smooth normal distributions, however it is clear that the total range is the same for both methods and Figure 6(b) shows a clear match in size distributions. In both cases the mean diameter differs by less than 2% when comparing manual and MATLAB measurements. Thus, reinforcing the results of the sensitivity analysis which indicates a maximum error of 10%.

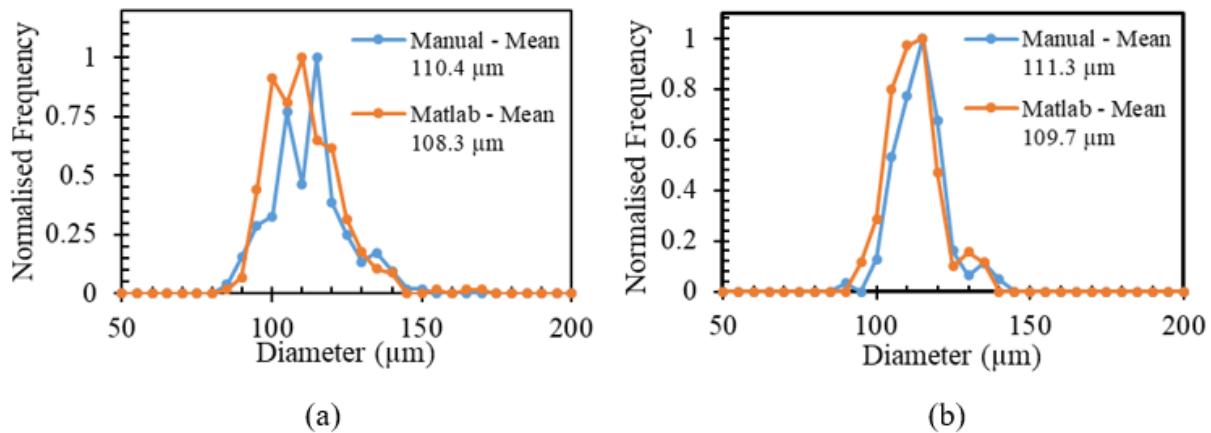


**Figure 6:** Size distribution and mean diameter obtained using manual image analysis and MATLAB analysis of seventeen different images from two different experimental runs (a) & (b) using threshold factors of Imbinarise = 0.75, Eccentricity = 0.5, 100-MinIntensity = 25.

### 335 **Effect of operating conditions**

336 Figure 7 shows the results testing at different pump operating conditions including inlet pressure,  
337 outlet pressure and water temperature. Baseline operating conditions of 0.3 MPa outlet pressure, -  
338 0.03 MPa inlet pressure, liquid flow rate of  $16.5 \text{ L min}^{-1}$  and an ambient air intake of  $1.5 \text{ L min}^{-1}$   
339 were used.

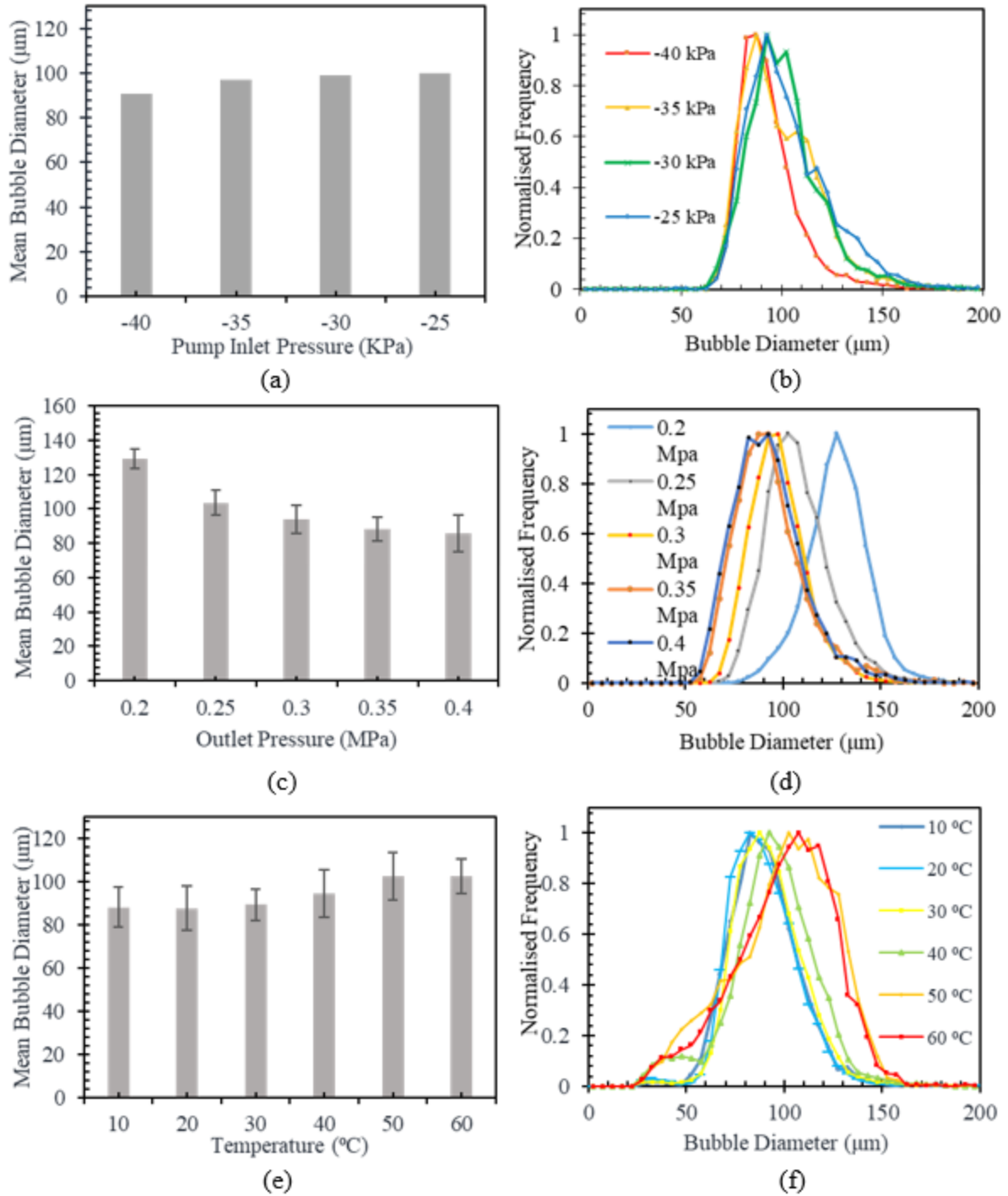


**Figure 7:** Mean diameter and size distribution of bubbles under various (a-b) pump inlet pressure, (c-d) pump outlet pressure, and (e-f) temperature . Error bars on plots represent the standard deviation of the mean diameter obtained from experimental repeats. Baseline operating parameters (0.3 MPa outlet pressure, -0.03 MPa inlet pressure, Temperature 20 C°)

Despite a slight increase in mean diameter as the magnitude of inlet pressure increased, there was no significant change in the mean MB diameter or size distribution when changing the inlet pressure, as the outlet/operating pressure within the pump was kept constant. At higher outlet/operating pressures, the size of the MBs produced by the pump decreased from 129  $\mu\text{m}$  to 86  $\mu\text{m}$ , well above any potential error from image analysis. Increased outlet pressure clearly allows smaller MBs to be produced. In the case of pressurisation/depressurisation type MB generation, an increased pressure and hence larger operating costs leads to smaller bubbles due to more gas being dissolved in the fluid and a larger pressure drop occurring over the injection nozzles [10]. In the case of the regenerative turbine pump used in this study, it is likely that smaller bubbles are produced due to increased shear forces within the pump because of higher localised pressure drops at vortices within the pump. At higher temperature, there was a slight increase in the average size of MB produced by the pump from 88  $\mu\text{m}$  to 102  $\mu\text{m}$ . The shift is more obvious when looking at the size distribution plots (Figure 6F) as the temperature increases. The total size distribution range remains the same, with peaks shifting towards larger bubble sizes. This increase in bubble size could be attributed to the expansion of air as it enters the pump. The set air flowrate of 1.5 l min<sup>-1</sup> is drawn at room temperature and therefore once exposed to higher temperatures inside the pump; the volume of air will increase due to thermal expansion. It is possible that MBs are fully formed within the pump prior to the gas temperature equilibrating with the water temperature, resulting in MB expansion after formation. It is also possible that a reduction in gas/liquid viscosity and surface tension could fundamentally alter the shear forces that lead to MB formation. Over the range of 10-60 °C, viscosity reduces by over 60% and surface tension reduced by over 10% (Table S2).

### **Effect of surfactant**

Surfactants reduce the surface tension of bubbles by the absorption of surfactant molecules onto the gas-liquid interface, with the hydrophobic surfactant moieties orientated towards the gas bubbles and the hydrophilic surfactant moieties orientated towards the bulk liquid. This results in enhanced bubble stability due to a reduction in bubble coalescence. Ionic surfactants CTAB (cationic) and GAELE (anionic) and non-ionic surfactants Triton X-100 and Tween 20 were used in this experiment. Due to foaming that occurred at higher proportions of the CMC there was an

upper limit for surfactant concentration. The results of the non-ionic surfactants, Triton X-100 and Tween 20 are shown in Figure 8.

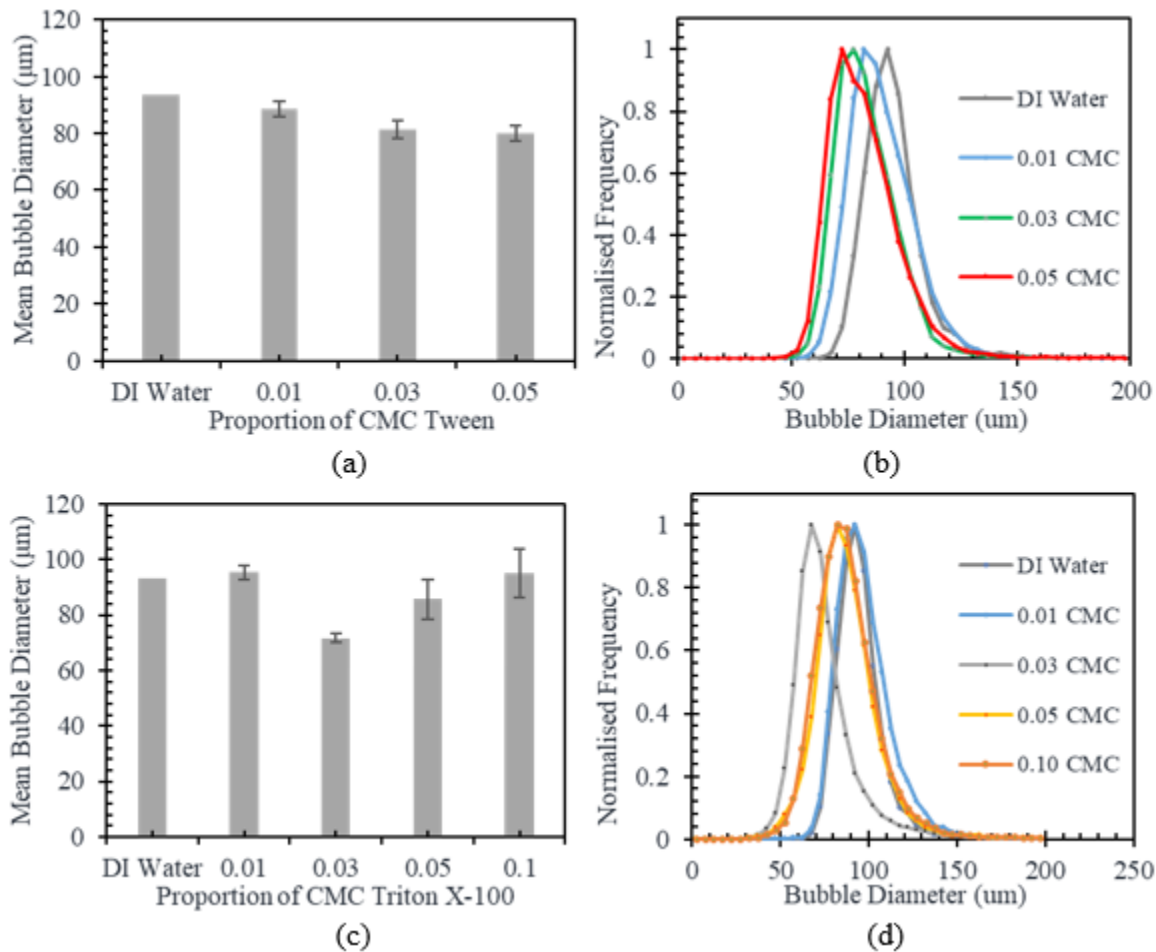


**Figure 8:** Mean diameter and size distributions of MBs produced at different proportions of CMC (critical micelle concentration) of Tween 20 (Top) and Triton X-100 (bottom). Error bars on plots represent standard deviation of the mean diameter obtained from experimental repeats.

The results for Tween 20 show a consistent trend in bubble diameter change, with the distribution shifting towards smaller diameters as surfactant concentration increases. Mean bubble diameter decreased as the proportion of critical micelle concentration (CMC) is increased to 0.05, with an overall reduction in mean size of from 93 μm to 79 μm. Tween 20 has previously been shown to be effective at reducing bubble size by an order of magnitude when using porous glass membrane for bubble generation [79]. In the case of Triton X-100 there was no discernible trend in bubble size with mean size fluctuating as surfactant concentration was increased. With Triton X-100

foaming was a significant problem even at lower proportions of the CMC. Use of ionic surfactants CTAB and GAELE exhibited significant reductions in bubble size (Figure 9). In both cases, there was a much larger drop in mean diameter than for the two non-ionic surfactants, from 90  $\mu\text{m}$  to 40  $\mu\text{m}$ . The difference between ionic and non-ionic surfactant suggests that surface charge is an important factor during bubble production within the pump, potentially reducing coalescence via increased repulsive forces between bubbles. This is supported by surface tension measurements that showed no significant variation at surfactant concentrations used, suggesting that surface charge effects alone are capable of reducing the mean bubble diameter. While no literature data for MB production in presence of GAELE was available, similar anionic surfactants have been tested, including sodium n-dodecylbenzene sulfonate [79] and sodium dodecal sulphate, with the latter showing bubble size reduction from 52  $\mu\text{m}$  to 30  $\mu\text{m}$  [80]. CTAB showed a larger reduction in bubble size at 0.01 CMC than GAELE. Previous literature has shown cationic surfactants has a greater effect at lower proportion CMC than anionic surfactants [81]. For cationic surfactants, a positive charge is applied to the surface and for anionic surfactants, a negative charge is applied to the surface [82]. Given that MBs generally have a negative surface charge in water, anionic surfactants will be repelled, while cationic surfactants would be attracted. This could cause cationic surfactants to adsorb at higher surface concentrations than anionic surfactants at low proportions of the CMC.

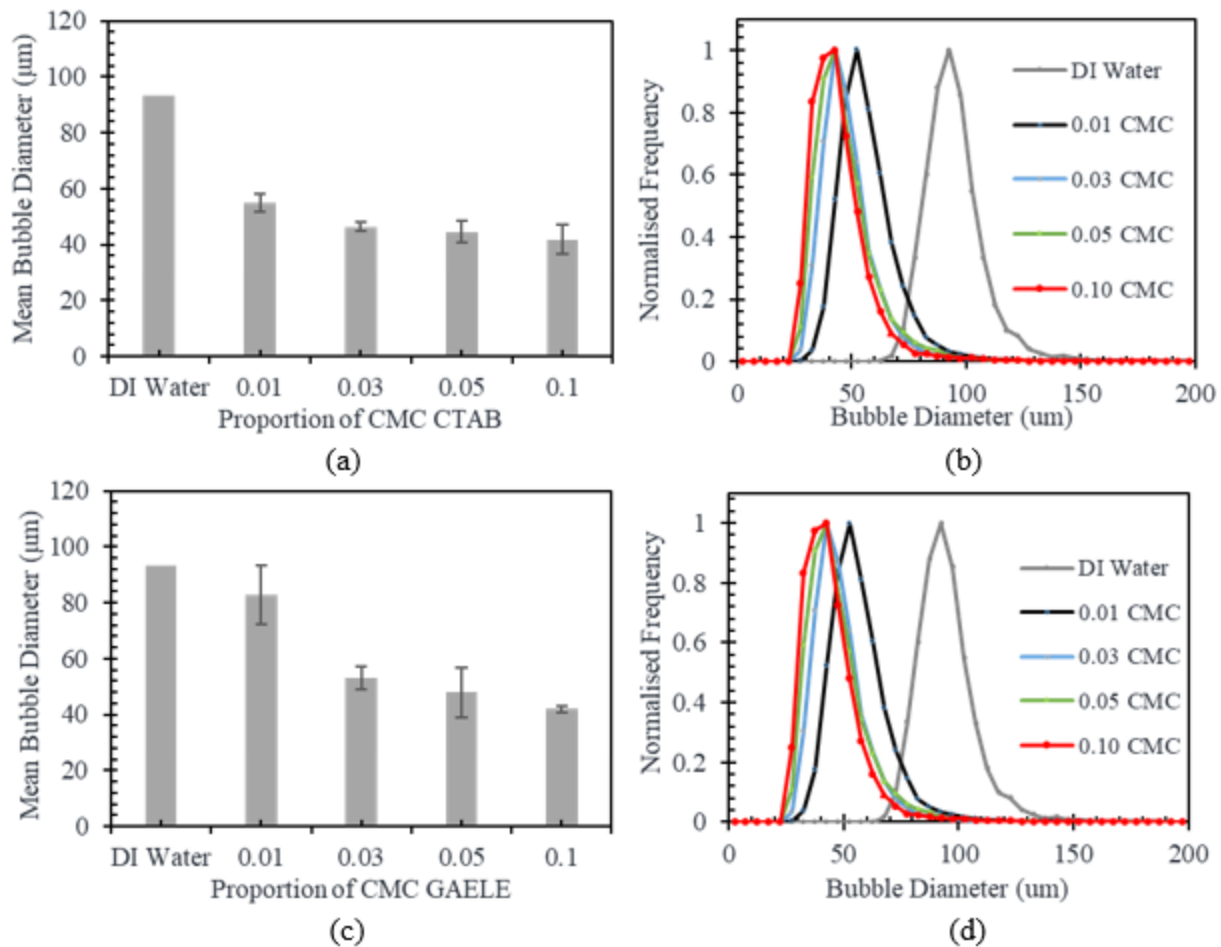


**Figure 9:** Mean diameter and size distributions of MBs produced at different proportions of CMC (critical micelle concentration) of CTAB (Top) and GAELE (bottom). Error bars on the plots represent standard deviation of the mean diameter obtained from experimental repeats.

### Rise Velocity

The rise velocity experiments were performed over a temperature range of 10 - 60 °C in DI water with three repeats for each temperature (Figure 9). Due to the high density of data points, outliers were eliminated by comparing points to the Stokes' law and retaining > 98% of all data with the best agreement. This was done to highlight that most data is located densely close to Stokes' prediction. Figures showing the deviation from Stokes' law for all data are presented in the Supporting Information. The rise velocity was shown to fit reasonably well with the predicted Stokes' velocity. This matches with the theory that the drag coefficient of small spherical bubbles overlaps with those of rigid spheres [69]. Although at higher temperatures, the rise velocity became



more scattered and spread out. This can be explained by the presence of significant instability, which was observed in the flow with turbulence being much more prevalent in the experimental runs at 60 C° where dynamic viscosity was half that at 20 C°.

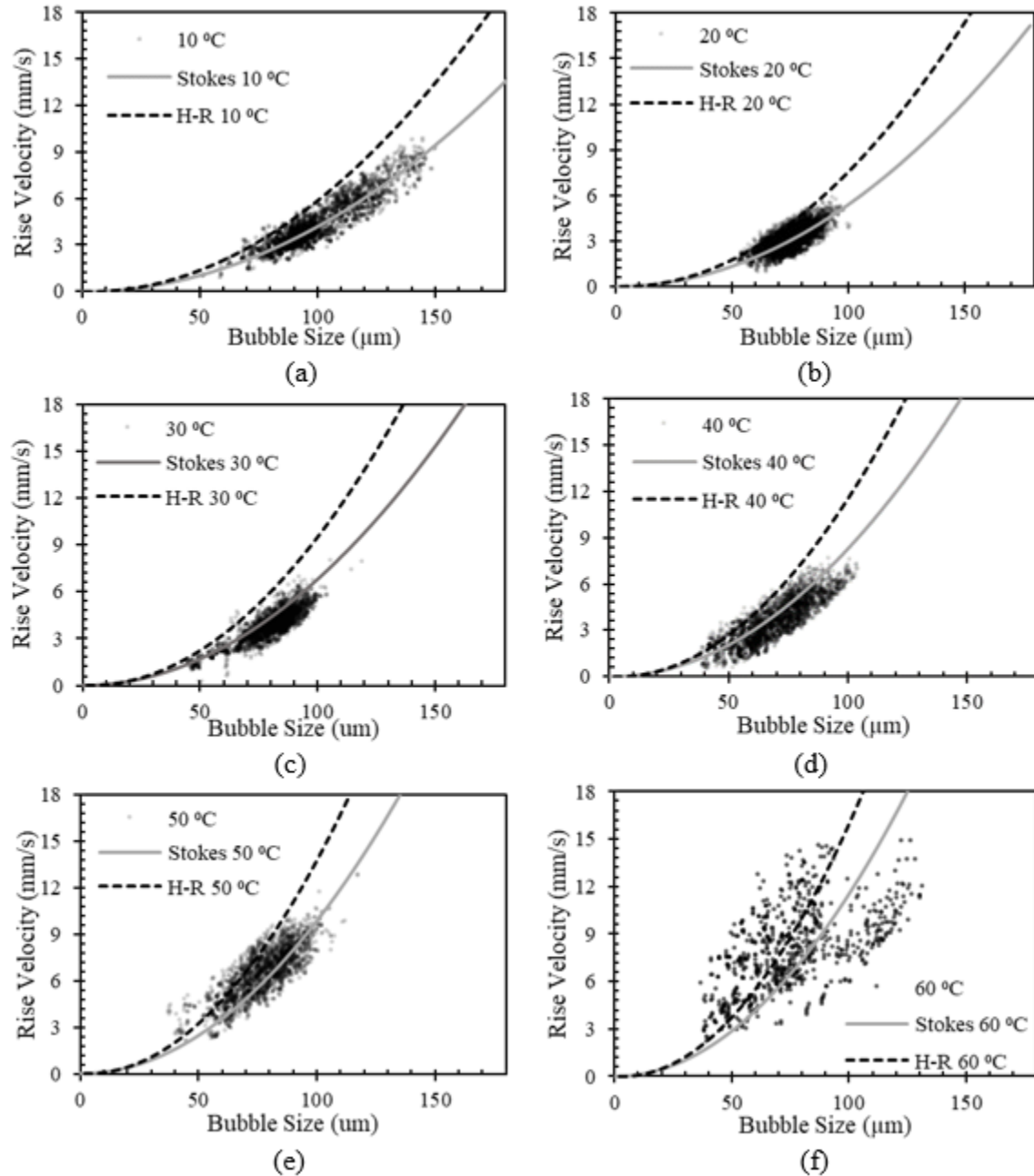


**Figure 10:** Rise velocity of MBs in DI water at different temperatures with Stokes' velocity (solid line) and the Hadamard-Rybczynski velocity (dashed line).

The  $Re_b$ ,  $Mo$  and  $Eo$  numbers were calculated for a bubble range of 1-150 μm, over 10 - 60°C, rising in water at Stokes' velocity as seen in Figure 11.  $Mo$  numbers were in the  $10^{-11}$  range. The

*Eo* number reached a value of 0.0033 at the maximum considered bubble size of 150  $\mu\text{m}$  and did not vary significantly with temperature, confirming that at such small bubble sizes the surface forces are dominant over the gravitational forces and that bubbles should maintain spherical. The maximum *Eo* value is also well below the Bond criterion cut-off of 4, suggesting that there is no internal circulation present within the MBs. The *Re<sub>b</sub>* number remained below 10 at all times but did exceed 1 for all temperature ranges. This suggests that certain bubbles at the higher end of the size distribution are expected to be excluded from the creeping flow regime and therefore exhibit rise velocities above the Stokes' prediction. The rise velocity plots obtained here do not exhibit this effect. Rise velocity matched with the Stokes' prediction. Experiments with larger bubbles could specify the transition of flow conditions.

Another factor to consider is the effect of bubble-bubble interactions on the rise velocity. High bubble volume fractions can lead to reduced rise velocities, whereas at lower volume fractions the rise velocity can be increased due to wake interactions. Here, bubble volume fractions were in the order of  $1 \times 10^{-3}$ , with a rise velocity assumed within 5% of the Stokes' prediction [83], while we observed higher deviations in some cases (SI, Figure S1). Substituting a bubble diameter of 100  $\mu\text{m}$ , bubble volume fraction of  $1 \times 10^{-3}$  and vessel diameter of 0.01 m into the Richardson-Zaki correlation [84] for particle sedimentation at  $\text{Re} < 0.2$  gives a rise velocity within 0.5% for a single bubble at terminal velocity (SI, Text S2). Significant reductions in rise velocity ( $>5\%$ ) are predicted at volume fraction an order of magnitude higher than used here. Future work should focus on the effect of bubble density and volume fraction on the observed rise velocity.

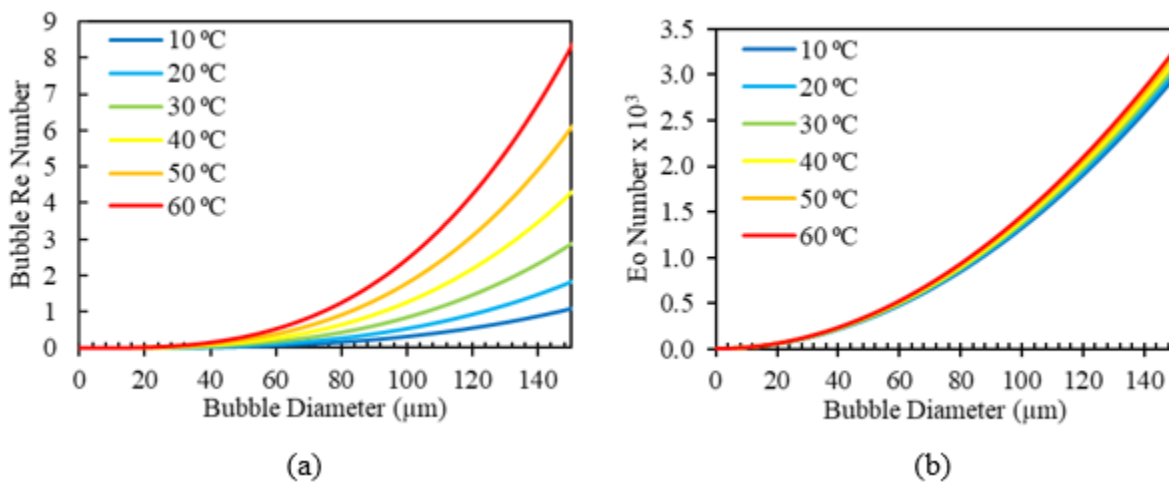


**Figure 11:** Plot of Reynolds and Eötvös numbers for bubbles rising at the predicted Stokes' velocity over a range of temperatures in RO water.

The effect of surfactant on rise velocity was also tested (Figure 12). The rise velocity matched well with the Stokes' prediction, including at higher temperatures. The match in rise velocity between experiments using DI water and experiments with added surfactants suggests that the surface of MBs is immobilised regardless of the presence of surfactants. This is in line with other studies showing that for bubbles under 300  $\mu\text{m}$ , the surface of the bubble can act like a solid even in clean liquids as a result of tangential shear stress caused by trace impurities [57], [68]. Previous research has shown that simply exposing the water used in the experimental system to unpurified atmospheric air, results in a decrease of the rise velocity from the Hadamard-Rybczynski prediction to a match of the Stokes' prediction [60]. As the MB generation setup in this research uses atmospheric air to generate MBs and is open to the atmosphere, it is therefore expected that bubbles behave according to Stokes' law.

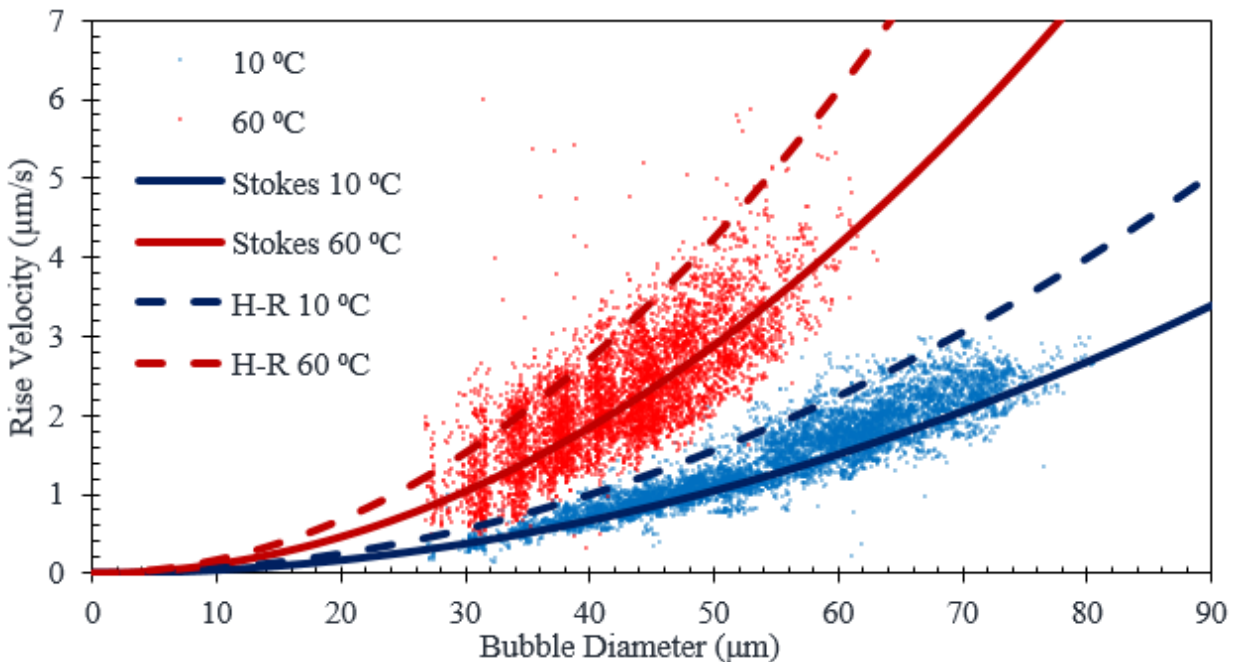


**Figure 12:** Rise velocity of bubbles in 0.01 CMC (critical micelle concentration) CTAB solution at 10 and 60 °C.

## Assumptions and Wider Applicability of Image Analysis Method

The image analysis method described has been designed and optimised for MB solutions such as found in DAF. Overlapping bubbles are ignored, while their effect on the obtained size distribution is assumed negligible. Similarly, non-circular shapes including overlapping bubbles are excluded. Hardware, solution conditions and the image analysis can be altered to meet different analytical challenges. For example, the analysis algorithm can be readily changed to account for different shapes including non-spheres, agglomerates and coalescing bubbles. With the employed equipment, imaging in the range of 20-150  $\mu\text{m}$  was easily achieved. For significantly smaller sizes ( $\ll 1 \mu\text{m}$ ) higher resolution and enhanced zoom capabilities are required. For bubble densities  $\gg 7 \text{ mm}^{-2}$  higher framerate collection may be required to track single bubbles. For analysis in opaque solutions the addition of contrasting agents, optical filters and further electronic image manipulation may be required to differentiate between liquid and bubbles. Ongoing work addresses the above areas to extend the capabilities of our system.

## 5. Conclusions

An automated image-based method to describe microbubbles in size, size distributions and rise velocities was developed. The method was tested with 50 – 150  $\mu\text{m}$  air microbubbles at densities of up to Stokes' bubbles /  $\text{mm}^2$  produced by a regenerative turbine pump with a water flowrate of 16  $\text{l min}^{-1}$  and an air flowrate of 1.5  $\text{l min}^{-1}$ . Series of bubble suspension images were collected from a side-stream viewing slit and processed through image analysis code that converted, filtered and statistically evaluated the initial images to yield both position and diameter of a subset of focussed bubbles within each image. The error of mean bubble size determined by the automated image analysis and manual evaluation was smaller than 2%. To show the ability of the method to detect small shifts in bubble size distribution, experiments were carried out over a range of operating conditions including pump pressure variation, water temperature variation and surfactant addition. Decreases in pump outlet pressure from 0.4 MPa to 0.2 MPa led to increasing mean bubble sizes from 86  $\mu\text{m}$  to 129  $\mu\text{m}$ . Temperature increase from 10  $^{\circ}\text{C}$  to 60  $^{\circ}\text{C}$  at an operating pressure of 0.3 MPa resulted in mean diameters increasing from 88  $\mu\text{m}$  to 102  $\mu\text{m}$ . Ionic surfactants reduced bubble size by 56%, in contrast to non-ionic surfactants, which had no significant effect on bubble size. Rise velocity analysis showed bubbles obeying Stokes' law for solid spheres moving through viscous fluid under creeping flow conditions irrespective of surfactant addition. Fast data processing allowed continuous measurements. Side stream sampling image analysis

497 provides scope for in-situ microbubble measurements and may be also applicable for  
498 characterising suspended solids.

## 499 **Supporting Information**

500 One text containing MATLAB codes, one table on results of sensitivity analysis, one figure on  
501 deviation of bubble rise velocity to Stokes' prediction, one figure on effect of calculating mean  
502 diameter with interquartile range (IQR) and Richardson-Zaki calculations.

## 503 **Nomenclature**

$c$	Numerical constant
$C_D$	Drag coefficient
$C_{DST}$	Stokes' drag coefficient
$D_b$	Bubble diameter
$Eo$	Eötvös number
$g$	Gravity
$Mo$	Morton number
$Re_b$	Bubble Reynolds number
$u_b$	Bubble rise velocity
$u_{t(ST)}$	Stokes' bubble terminal rise velocity
$u_{t(H-R)}$	Hadamard-Rybczynski bubble terminal rise velocity
$w$	$\log_{10} Re_b$
$\gamma$	Surface tension
$\mu_l$	Liquid viscosity
$\mu_g$	Gas viscosity
$\rho_l$	Liquid density
$\rho_g$	Gas density
$\Delta\rho$	$\rho_l - \rho_g$

504

## 505 **Acknowledgements.**

506 B.S was supported by a scholarship of the Water Informatics, Science and Engineering (WISE)  
507 Centre for Doctoral Training (CDT), funded by the UK Engineering and Physical Sciences  
508 Research Council, Grant No. EP/L016214/1. We thank Peter Pridham for valuable discussions.

## 509 **References**

- 510 [1] Y. Wibisono, E. R. Cornelissen, A. J. B. Kemperman, W. G. J. van der Meer, and K.  
511 Nijmeijer, "Two-phase flow in membrane processes: A technology with a future," *J.*  
512 *Memb. Sci.*, vol. 453, pp. 566–602, Mar. 2014.
- 513 [2] S. Khuntia, S. K. Majumder, and P. Ghosh, "Microbubble-aided water and wastewater  
514 purification: a review," *Rev. Chem. Eng.*, vol. 28, no. 4–6, pp. 191–221, Jan. 2012.
- 515 [3] A. Agarwal, W. J. Ng, and Y. Liu, "Principle and applications of microbubble and  
516 nanobubble technology for water treatment," *Chemosphere*, vol. 84, no. 9, pp. 1175–1180,  
517 Aug. 2011.
- 518 [4] R. T. Rodrigues and J. Rubio, "DAF–dissolved air flotation: Potential applications in the  
519 mining and mineral processing industry," *Int. J. Miner. Process.*, vol. 82, no. 1, pp. 1–13,  
520 Feb. 2007.
- 521 [5] E. Germain and T. Stephenson, "Biomass characteristics, aeration and oxygen transfer in  
522 membrane bioreactors: Their interrelations explained by a review of aerobic biological  
523 processes," *Reviews in Environmental Science and Biotechnology*, vol. 4, no. 4, pp. 223–  
524 233, Nov-2005.
- 525 [6] G. Q. Yang, B. Du, and L. S. Fan, "Bubble formation and dynamics in gas-liquid-solid  
526 fluidization-A review," *Chem. Eng. Sci.*, vol. 62, no. 1–2, pp. 2–27, Jan. 2007.
- 527 [7] "ISO - ISO/TC 281 - Fine bubble technology." [Online]. Available:  
528 <https://www.iso.org/committee/4856666.html>. [Accessed: 07-Apr-2020].
- 529 [8] M. Takahashi, K. Chiba, and P. Li, "Free-radical generation from collapsing microbubbles  
530 in the absence of a dynamic stimulus," *The Journal of Physical Chemistry B*, vol. 111, no.  
531 6, pp. 1343-1347, Jan. 2007.
- 532 [9] H. Tsuge, *Micro- and nanobubbles : Fundamentals and applications*. 1<sup>st</sup> ed. Jenny  
533 Stanford Publishing, CRC Press, 2015.
- 534 [10] J. K. Edzwald, "Dissolved air flotation and me," *Water Res.*, vol. 44, no. 7, pp. 2077–  
535 2106, Apr. 2010.
- 536 [11] T. Temesgen, T. T. Bui, M. Han, T. Kim, and H. Park, "Micro and nanobubble  
537 technologies as a new horizon for water-treatment techniques: A review," *Adv. Colloid*  
538 *Interface Sci.*, vol. 246, pp. 40–51, Aug. 2017.
- 539 [12] G. Z. Kyzas and K. A. Matis, "Electroflotation process: A review," *J. Mol. Liq.*, vol. 220,  
540 pp. 657–664, Aug. 2016.
- 541 [13] J. K. Edzwald, *Water Quality & Treatment*, 6th ed. 2011.
- 542 [14] H. Ikeura, F. Kobayashi, and M. Tamaki, "Removal of residual pesticide, fenitrothion, in  
543 vegetables by using ozone microbubbles generated by different methods," *J. Food Eng.*,  
544 vol. 103, no. 3, pp. 345–349, Apr. 2011.
- 545 [15] T. Zheng, Q. Wang, T. Zhang, Z. Shi, Y. Tian, S. Shi, N. Smale, and J. Wang,

546 “Microbubble enhanced ozonation process for advanced treatment of wastewater  
547 produced in acrylic fiber manufacturing industry,” *J. Hazard. Mater.*, vol. 287, pp. 412–  
548 420, Apr. 2015.

549 [16] W. B. Zimmerman, M. Zandi, H. C. Hemaka Bandulasena, V. Tesař, D. James Gilmour,  
550 and K. Ying, “Design of an airlift loop bioreactor and pilot scales studies with fluidic  
551 oscillator induced microbubbles for growth of a microalgae *Dunaliella salina*,” *Appl.*  
552 *Energy*, vol. 88, no. 10, pp. 3357–3369, Oct. 2011.

553 [17] L.-B. Chu, S.-T. Yan, X.-H. Xing, A.-F. Yu, X.-L. Sun, and B. Jurcik, “Enhanced sludge  
554 solubilization by microbubble ozonation,” *Chemosphere*, vol. 72, no. 2, pp. 205–212, May  
555 2008.

556 [18] K. Terasaka, A. Hirabayashi, T. Nishino, S. Fujioka, and D. Kobayashi, “Development of  
557 microbubble aerator for waste water treatment using aerobic activated sludge,” *Chem.*  
558 *Eng. Sci.*, vol. 66, no. 14, pp. 3172–3179, Jul. 2011.

559 [19] M. Miyamoto, S. Ueyama, N. Hinomoto, T. Saitoh, S. Maekawa, and J. Hirotsuji,  
560 “Degreasing of Solid Surfaces by Microbubble Cleaning,” *Jpn. J. Appl. Phys.*, vol. 46, no.  
561 3A, pp. 1236–1243, Mar. 2007.

562 [20] N. Ahmed and G. J. Jameson, “The effect of bubble size on the rate of flotation of fine  
563 particles,” *Int. J. Miner. Process.*, vol. 14, no. 3, pp. 195–215, Apr. 1985.

564 [21] B. V. Derjaguin, S. S. Dukhin, and N. N. Rulyov, “Kinetic Theory of Flotation of Small  
565 Particles,” in *Surface and Colloid Science*, Boston, MA: Springer US, 1984, pp. 71–113.

566 [22] P. Diaz-Penafiel and G. S. Dobby, “Kinetic studies in flotation columns: Bubble size  
567 effect,” *Miner. Eng.*, vol. 7, no. 4, pp. 465–478, Apr. 1994.

568 [23] J. K. Edzwald, “Principles and applications of dissolved air flotation,” *Water Sci.*  
569 *Technol.*, vol. 31, no. 3–4, 1995.

570 [24] L. R. Flint and W. J. Howarth, “The collision efficiency of small particles with spherical  
571 air bubbles,” *Chem. Eng. Sci.*, vol. 26, no. 8, pp. 1155–1168, Aug. 1971.

572 [25] D. Reay and G. A. Ratcliff, “Removal of fine particles from water by dispersed air  
573 flotation: Effects of bubble size and particle size on collection efficiency,” *Can. J. Chem.*  
574 *Eng.*, vol. 51, no. 2, pp. 178–185, Apr. 1973.

575 [26] M. D. Bredwell and R. M. Worden, “Mass-Transfer Properties of Microbubbles. 1.  
576 Experimental Studies,” *Biotechnol. Prog.*, vol. 14, no. 1, pp. 31–38, Feb. 1998.

577 [27] S. Waslo and B. Gal-or, “Boundary layer theory for mass and heat transfer in clouds of  
578 moving drops, bubbles or solid particles,” *Chem. Eng. Sci.*, vol. 26, no. 6, pp. 829–838,  
579 Jun. 1971.

580 [28] R. M. Worden and M. D. Bredwell, “Mass-Transfer Properties of Microbubbles. 2.  
581 Analysis Using a Dynamic Model,” *Biotechnol. Prog.*, vol. 14, no. 1, pp. 39–46, Feb.  
582 1998.

- 583 [29] W. E. Juwana, A. Widyatama, O. Dinaryanto, W. Budhijanto, Indarto, and Deendarlianto,  
584 "Hydrodynamic characteristics of the microbubble dissolution in liquid using orifice type  
585 microbubble generator," *Chem. Eng. Res. Des.*, vol. 141, pp. 436–448, Jan. 2019.
- 586 [30] X. Li, P. Li, L. Zu, and C. Yang, "Gas-Liquid Mass Transfer Characteristics with  
587 Microbubble Aeration - I. Standard Stirred Tank," *Chem. Eng. Technol.*, vol. 39, no. 5, pp.  
588 945–952, May 2016.
- 589 [31] A. Amaral, G. Bellandi, U. Rehman, R. Neves, Y. Amerlinck, and I. Nopens, "Towards  
590 improved accuracy in modeling aeration efficiency through understanding bubble size  
591 distribution dynamics," 2017.
- 592 [32] A. A. Kulkarni and J. B. Joshi, "Bubble formation and bubble rise velocity in gas-liquid  
593 systems: A review," *Industrial and Engineering Chemistry Research*, vol. 44, no. 16. pp.  
594 5873–5931, 03-Aug-2005.
- 595 [33] W. A. Ducker, Z. Xu, and J. N. Israelachvili, "Measurements of Hydrophobic and DLVO  
596 Forces in Bubble-Surface Interactions in Aqueous Solutions," *Langmuir*, vol. 10, no. 9,  
597 pp. 3279–3289, Sep. 1994.
- 598 [34] M. Han and S. Dockko, "Zeta potential measurement of bubbles in DAF process and its  
599 effect on the removal efficiency," *KSCE J. Civ. Eng.*, vol. 2, no. 4, pp. 461–466, Dec.  
600 1998.
- 601 [35] S. Dockko and M. Y. Han, "Fundamental characteristics of bubbles and ramifications for  
602 the flotation process," *Water Sci. Technol.*, vol. 50, no. 12, pp. 207–214, Dec. 2004.
- 603 [36] M. Han, T. Kim, and J. Kim, "Effects of floc and bubble size on the efficiency of the  
604 dissolved air flotation (DAF) process," *Water Sci. Technol.*, vol. 56, no. 10, pp. 109–115,  
605 Nov. 2007.
- 606 [37] M. Takahashi, "ζ Potential of Microbubbles in Aqueous Solutions: Electrical Properties of  
607 the Gas–Water Interface," *J. Phys. Chem. B*, vol. 109, no. 46, pp. 21858–21864, Nov.  
608 2005.
- 609 [38] I. U. Vakarelski R. Manica, X. Tang, S. J. O'Shea, G. W. Stevens, F. Grieser, R. R.  
610 Dagastine, and D. Y. C. Chan, "Dynamic interactions between microbubbles in water.,"  
611 *Proc. Natl. Acad. Sci. U. S. A.*, vol. 107, no. 25, pp. 11177–82, Jun. 2010.
- 612 [39] S. Tanaka, S. Kastens, S. Fujioka, M. Schlüter, and K. Terasaka, "Mass transfer from  
613 freely rising microbubbles in aqueous solutions of surfactant or salt," *Chem. Eng. J.*, Mar.  
614 2019.
- 615 [40] M. Y. Han, "Modeling of DAF: the effect of particle and bubble characteristics," *J. Water  
616 Supply Res. Technol.*, vol. 51, no. 1, pp. 27–34, Feb. 2002.
- 617 [41] R. M. Griffith, "The effect of surfactants on the terminal velocity of drops and bubbles,"  
618 *Chem. Eng. Sci.*, vol. 17, no. 12, pp. 1057–1070, Dec. 1962.
- 619 [42] S. S. Alves, S. P. Orvalho, and J. M. T. Vasconcelos, "Effect of bubble contamination on



620 rise velocity and mass transfer,” *Chem. Eng. Sci.*, vol. 60, no. 1, pp. 1–9, Jan. 2005.

621 [43] S. Takagi and Y. Matsumoto, “Surfactant Effects on Bubble Motion and Bubbly Flows,”  
622 *Annu. Rev. Fluid Mech.*, vol. 43, no. 1, pp. 615–636, Jan. 2011.

623 [44] R. Bel Fdhila and P. C. Duineveld, “The effect of surfactant on the rise of a spherical  
624 bubble at high Reynolds and Peclet numbers,” *Phys. Fluids*, vol. 8, no. 2, pp. 310–321,  
625 Feb. 1996.

626 [45] S. S. Sadhal and R. E. Johnson, “Stokes flow past bubbles and drops partially coated with  
627 thin films. Part 1. Stagnant cap of surfactant film – exact solution,” *J. Fluid Mech.*, vol.  
628 126, no. 1, p. 237, Jan. 1983.

629 [46] C. T. Ta, J. Beckley, and A. Eades, “A multiphase CFD model of DAF process,” *Water  
630 Sci. Technol.*, vol. 43, no. 8, pp. 153–7, 2001.

631 [47] J. Hague, C. T. Ta, M. J. Biggs, and J. A. Sattary, “Small scale model for CFD validation  
632 in DAF application,” *Water Sci. Technol.*, vol. 43, no. 8, pp. 167–173, Apr. 2001.

633 [48] M. Kostoglou, T. D. Karapantsios, and K. A. Matis, “CFD Model for the Design of Large  
634 Scale Flotation Tanks for Water and Wastewater Treatment,” 2007.

635 [49] T. Amato and J. Wicks, “The practical application of computational fluid dynamics to  
636 dissolved air flotation, water treatment plant operation, design and development,” *J. Water  
637 Supply Res. Technol. - AQUA*, vol. 58, no. 1, pp. 65–73, 2009.

638 [50] A. Chen, Z. Wang, and J. Yang, “Influence of bubble size on the fluid dynamic behavior  
639 of a DAF tank: A 3D numerical investigation,” *Colloids Surfaces A Physicochem. Eng.  
640 Asp.*, vol. 495, pp. 200–207, Apr. 2016.

641 [51] B. Lakghomi, Y. Lawryshyn, and R. Hofmann, “Evaluation of flow hydrodynamics in a  
642 pilot-scale dissolved air flotation tank: a comparison between CFD and experimental  
643 measurements,” *Water Sci. Technol.*, vol. 72, no. 7, p. 1111, Sep. 2015.

644 [52] D. M. Leppinen and S. B. Dalziel, “Bubble size distribution in dissolved air flotation  
645 tanks,” *J. Water Supply Res. Technol. - Aqua*, vol. 53, no. 8, 2004.

646 [53] E. M. Rykaart and J. Haarhoff, “Behaviour of air injection nozzles in dissolved air  
647 flotation,” *Water Sci. Technol.*, vol. 31, no. 3–4, pp. 25–35, Feb. 1995.

648 [54] M. Li, A. Bussonnière, M. Bronson, Z. Xu, and Q. Liu, “Study of Venturi tube geometry  
649 on the hydrodynamic cavitation for the generation of microbubbles,” *Miner. Eng.*, vol.  
650 132, pp. 268–274, Mar. 2019.

651 [55] H. Ohnari, “System and method for generating gas micro-bubbles in a liquid” *European  
652 Patent Office* EP1112773B1, 15-May-2000..

653 [56] F. Rehman, G. J. D. Medley, H. Bandulasena, and W. B. J. Zimmerman, “Fluidic  
654 oscillator-mediated microbubble generation to provide cost effective mass transfer and  
655 mixing efficiency to the wastewater treatment plants,” *Environ. Res.*, vol. 137, pp. 32–39,

- 656 Feb. 2015.
- 657 [57] L. Parkinson, R. Sedev, D. Fornasiero, and J. Ralston, "The terminal rise velocity of 10–  
658 100  $\mu\text{m}$  diameter bubbles in water," *J. Colloid Interface Sci.*, vol. 322, no. 1, pp. 168–172,  
659 Jun. 2008.
- 660 [58] A. Eskinlou, M. R. Khalesi, M. Mirmogaddam, M. Hemmati Chegeni, and B. Vaziri  
661 Hassas, "Investigation of trajectory and rise velocity of loaded and bare single bubbles in  
662 flotation process using video processing technique," *Sep. Sci. Technol.*, pp. 1–8, Oct.  
663 2018.
- 664 [59] D. H. Kwak, H. J. Jung, S. B. Kwon, E. J. Lee, C. H. Won, J. W. Lee, and S. J. Yoo, "Rise  
665 velocity verification of bubble-floc agglomerates using population balance in the DAF  
666 process," *J. Water Supply Res. Technol.*, vol. 58, no. 2, p. 85, Mar. 2009.
- 667 [60] G. H. Kelsall, S. Tang, A. L. Smith, and S. Yurdakul, "Measurement of rise and  
668 electrophoretic velocities of gas bubbles," *J. Chem. Soc. Faraday Trans.*, vol. 92, no. 20,  
669 p. 3879, Jan. 1996.
- 670 [61] M. Y. Han, Y. H. Park, and T. J. Yu, "Development of a new method of measuring bubble  
671 size," *Water Sci. Technol. Water Supply*, vol. 2, no. 2, pp. 77–83, Apr. 2002.
- 672 [62] S. J. Gulden, C. Riedele, S. Rollie, M.-H. Kopf, and H. Nirschl, "Online bubble size  
673 analysis in micro flotation," *Chem. Eng. Sci.*, vol. 185, pp. 168–181, Aug. 2018.
- 674 [63] S. E. de Rijk, G. Jaap H.J.M. der Aivan, and J. G. den Blanken, "Bubble size in flotation  
675 thickening," *Water Res.*, vol. 28, no. 2, pp. 465–473, Feb. 1994.
- 676 [64] L. O. Filippov, R. Joussemet, and R. Houot, "Bubble spargers in column flotation:  
677 Adaptation to precipitate flotation," *Miner. Eng.*, vol. 13, no. 1, pp. 37–51, Jan. 2000.
- 678 [65] W. Kracht, X. Emery, and C. Paredes, "A stochastic approach for measuring bubble size  
679 distribution via image analysis," *Int. J. Miner. Process.*, vol. 121, pp. 6–11, Jun. 2013.
- 680 [66] R. Grau and K. Heiskanen, "Visual technique for measuring bubble size in flotation  
681 machines," *Miner. Eng.*, vol. 15, no. 7, pp. 507–513, Jul. 2002.
- 682 [67] L. Vinnett, J. Sovechles, C. O. Gomez, and K. E. Waters, "An image analysis approach to  
683 determine average bubble sizes using one-dimensional Fourier analysis," *Miner. Eng.*, vol.  
684 126, pp. 160–166, Sep. 2018.
- 685 [68] R. Clift, J. R. Grace, and M. E. Weber, "Shapes of Rigid and Fluid Particles," in *Bubbles,*  
686 *drops, and particles*, Academic Press, 1978, p. 380.
- 687 [69] M. Pfister, W. H. Hager, and F. Asce, "History and Significance of the Morton Number in  
688 Hydraulic Engineering," 2014.
- 689 [70] R. Clift, J. R. Grace, and M. E. Weber, "Spheres at Higher Reynolds Numbers," in  
690 *Bubbles, drops, and particles*, Academic Press, 1978, p. 380.
- 691 [71] R. Clift, J. R. Grace, and M. E. Weber, "Slow Viscous Flow Past Spheres," in *Bubbles,*

- 692        *drops, and particles*, Academic Press, 1978, p. 380.
- 693    [72]    W. N. Bond and D. A. Newton, “Bubbles, drops, and Stokes’ law. (Paper 2),” *London,*  
694        *Edinburgh, Dublin Philos. Mag. J. Sci.*, vol. 5, no. 30, pp. 794–800, Apr. 1928.
- 695    [73]    R. Clift, J. R. Grace, and M. E. Weber, *Bubbles, drops, and particles*. Academic Press,  
696        1978.
- 697    [74]    J. Haarhoff and J. K. Edzwald, “Dissolved air flotation modelling: insights and  
698        shortcomings,” *J. Water Supply Res. Technol. - Aqua*, vol. 53, no. 3, 2004.
- 699    [75]    Y. Matsui, K. Fukushi, and N. Tambo, “Modeling, simulation and operational parameters  
700        of dissolved air flotation,” *J. Water Supply Res. Technol. - Aqua*, vol. 47, no. 1, 1998.
- 701    [76]    A. Loisy, A. Naso, and P. D. M. Spelt, “Buoyancy-driven bubbly flows: ordered and free  
702        rise at small and intermediate volume fraction,” *J. Fluid Mech.*, p. 816, 2017.
- 703    [77]    P. W. Pridham, “Nikuni KTM Microbubble Generating Pump Operating Instructions.”  
704        2015.
- 705    [78]    N. Otsu, “Threshold selection method from gray-level histograms” *IEEE Trans Syst Man*  
706        *Cybern*, vol. SMC-9, no. 1, pp. 62–66, 1979..
- 707    [79]    M. Kukizaki and Y. Baba, “Effect of surfactant type on microbubble formation behavior  
708        using Shirasu porous glass (SPG) membranes,” *Colloids Surfaces A Physicochem. Eng.*  
709        *Asp.*, vol. 326, no. 3, pp. 129–137, Sep. 2008.
- 710    [80]    R. Parmar and S. K. Majumder, “Terminal rise velocity, size distribution and stability of  
711        microbubble suspension,” *Asia-Pacific J. Chem. Eng.*, vol. 10, no. 3, pp. 450–465, May  
712        2015.
- 713    [81]    H. J. B. Couto, D. G. Nunes, R. Neumann, and S. C. A. França, “Micro-bubble size  
714        distribution measurements by laser diffraction technique,” *Miner. Eng.*, vol. 22, no. 4, pp.  
715        330–335, Mar. 2009.
- 716    [82]    A. Bueno-Tokunaga, R. Pérez-Garibay, and D. Martínez-Carrillo, “Zeta potential of air  
717        bubbles conditioned with typical froth flotation reagents,” *Int. J. Miner. Process.*, vol.  
718        140, pp. 50–57, Jul. 2015.
- 719    [83]    A. S. Sangani, “Sedimentation in ordered emulsions of drops at low Reynolds numbers,”  
720        *ZAMP Zeitschrift für Angew. Math. und Phys.*, vol. 38, no. 4, pp. 542–556, Jul. 1987.
- 721    [84]    J. F. Richardson and W. N. Zaki, “Sedimentation and fluidization: Part I,” *Process Saf.*  
722        *Environ. Prot. Trans. Inst. Chem. Eng. Part B*, vol. 75, no. Suppl, pp. S82–S100, Dec.  
723        1997.

724